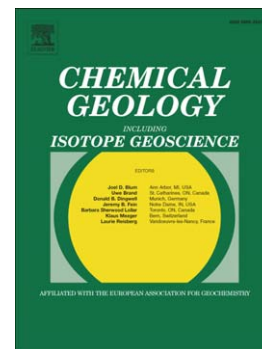# Accepted Manuscript

Accurate analysis of shallowly implanted solar wind ions by SIMS backside depth profiling

Veronika S. Heber, Kevin D. McKeegan, Donald S. Burnett, Jean Duprat, Yunbin Guan, Amy Jurewicz, Chad T. Olinger, Stephen P. Smith

Please cite this article as: Heber, Veronika S., McKeegan, Kevin D., Burnett, Donald S., Duprat, Jean, Guan, Yunbin, Jurewicz, Amy, Olinger, Chad T., Smith, Stephen P., Accurate analysis of shallowly implanted solar wind ions by SIMS backside depth profiling, *Chemical Geology* (2014), doi: 10.1016/j.chemgeo.2014.10.003

Accurate analysis of shallowly implanted solar wind ions by

SIMS backside depth profiling

by

Veronika S. Heber[a,b,c], Kevin D. McKeegan[a], Donald S. Burnett[d], Jean Duprat[e], Yunbin Guan[d], Amy

Jurewicz[f], Chad T. Olinger[g], and Stephen P. Smith[h].

[a] Department of Earth, Planetary, and Space Sciences, UCLA, Los Angeles, CA, USA, 90095-1567; veronika.heber@psi.ch

[b] Visiting Scientist, Department of Earth Sciences, ETH Zurich, Switzerland

[c] present address: Paul Scherrer Institute, Division for Radiation Safety and Security, 5232 Villigen PSI, Switzerland

[d] California Institute of Technology, Pasadena, CA, USA

[e] CSNSM, CNRS/IN2P3-Univ. Paris Sud, Bat 104, F-91405 Orsay, France

[f] Arizona State University, Tempe, AZ, USA

[g] Applied Modern Physics, Los Alamos National Laboratory, Los Alamos, USA

[h] Evans Analytical Group, Sunnyvale, CA, USA

ABSTRACT

A method to quantitatively determine the fluences of shallowly-implanted solar wind ions returned to Earth by the Genesis Discovery mission is described. Through backside depth-profiling, we recover nearly complete depth profiles of implanted solar wind for several nonvolatile elements, including Mg, Al, Ca, Cr, and to a lesser extent, Na, in silicon targets that collected bulk solar wind and solar wind from specific velocity regimes. We also determine fluences of the volatile elements C, N, and O in silicon targets that collected bulk solar wind. By use of appropriately calibrated ion implanted standards, fluences as low as 2×10^{10} atoms cm^{-2} can be determined with precision and accuracy typically in the few percent range. Specific approaches to sample preparation, sputtering artifacts during depth profiling by secondary ion mass spectrometry, and quantification including production of ion implant standards are discussed.

1. Introduction

NASA Discovery Mission V, Genesis, collected solar wind in space, 1.5 million km sunward from Earth, for a period of 2.3 years and returned this sample for laboratory analysis (Burnett et al., 2003; Burnett and Team, 2011; Reisenfeld et al., 2013). The solar wind can serve as a proxy for the composition of the Sun and, thus, average of composition of the solar nebula (Marty et al., 2011; McKeegan et al., 2011), provided that fractionation processes occurring during the formation of the solar wind (e.g., Heber et al., 2012a) can be understood and quantitatively modeled. The objective of the Genesis mission is to obtain elemental and isotopic abundances of elements heavier than helium in the solar wind with precisions and accuracies better than those available from spacecraft data, which have uncertainties on the order of up to several tens of percent (e.g., Giammanco et al., 2008; von Steiger et al., 2000).

The solar wind at 1 AU (astronomical unit) is comprised of plasma with ion speeds of about 400 km s^{-1}, equivalent to a mean particle energy of ~1 keV per amu (atomic mass unit). This enables solar wind ions to penetrate, i.e. implant, into exposed collectors that are high purity semiconductor materials (e.g., silicon wafer, diamond-like carbon, sapphire; (Jurewicz et al., 2003)). The implantation results in a depth distribution of the solar wind ions in the collectors that peaks at ~40 nm and a tails up to a few hundreds of nanometers. The solar wind is comprised of ~96 atom% hydrogen, ~4 atom% helium, with all heavier elements occurring as minor or trace species in roughly solar abundances, e.g., 0.05 atom% oxygen and 3 ppma (parts per million atomic) aluminum (Asplund et al., 2009). Thus, the analytical challenge for Genesis is to accurately measure these low-abundance species with precision useful for planetary science (Burnett and Team, 2011), a challenge made more difficult by the shallow depth of the implanted solar wind. Despite the excellent purity of the collector materials themselves, the terrestrial contamination on their surfaces is significant. Terrestrial contamination varies among collectors sampled

3

and can include: a natural oxide layer (complicating oxygen analyses), a molecular film deposited in space by outgassing of organic compounds and subsequent UV polymerization (Allton et al., 2006), and particulates (e.g., soil, salt, pulverized collectors) deposited during the hard landing of the science canister in the Utah desert in September 2004.

For elements other than noble gases, the most widely used method to extract and analyze the implanted solar wind is depth profiling by secondary ion mass spectrometry (SIMS) (e.g., Heber et al., 2013; Heber et al., 2014; Huss et al., 2012; Marty et al., 2011; McKeegan et al., 2011; Rieck et al., 2014). The SIMS method is extensively employed in the semiconductor industry to analyze in-depth distributions of dopant elements (e.g., Wilson et al., 1989; Zinner, 1983). The high depth resolution achieved by SIMS, in principle, enables the separation of surface contamination from the ion implant. The ion microscope capability of the Cameca IMS 1270 (UCLA) and 7f-Geo (CalTech) SIMS instruments employed in this work allows insertion of a field aperture in an image plane thus restricting collection of secondary ions to only the center of a sputtered pit and minimizing contributions from the crater walls. In addition, the ion imaging capability allows the detection of micron-sized contaminant particles on the sample surface so that they can then be avoided.

Despite the excellent depth resolution inherent in secondary ion formation by sputtering, and even considering the restriction of accepted ions from the instantaneous crater bottom enabled by the ion microscope, the extremely low solar wind fluences of elements implanted in the Genesis targets (e.g., ~9.7 x 10^{10} atoms cm^{-2} for sodium in the bulk solar wind collector, see Fig. 10) coupled with the shallow penetration depths and ubiquitous surface contamination make quantitative analysis of the solar wind profiles highly problematic by conventional SIMS depth-profiling. For example, atomic mixing and knock-on of ions from a high-abundance surface contaminant to the low concentration region of solar wind can partially or entirely mask the signal of interest; this problem is especially acute for the volatile

elements carbon, nitrogen, and oxygen that comprise residual vacuum species and which are often components of surface films on Genesis collectors (see for nitrogen Huss et al., 2012). The degradation of depth resolution by the addition of these knocked-on ions may result in erroneously high solar wind fluences or incorrect isotopic compositions. A further problem for quantitation of ion signals in the very near surface layers results from preferential sputtering effects, a problem long recognized in the semiconductor industry (e.g., see review by Zinner, 1983). At the beginning of the sputter process (or at any sharp interface of changing target composition), secondary ion yields vary markedly. The effect is particularly strong when sputtering with reactive ion beams (e.g., cesium or oxygen) that are used to enhance secondary ion formation (and, thus, sensitivity). The nonequilibrium sputtering effects scale with implantation depth of the primary ion beam (Wilson et al., 1989), and even under favorable conditions (e.g., low impact energy) correspond to depths of typically up to ~10 nm in the ion microscope instruments considered here. For some elements, certain "tricks", such as low impact energy primary ion beams and/or gaseous oxygen flooding of the sample analysis area, can be used to minimize ion beam mixing of surface contamination and transient effects on SIMS ion yields due to preferential sputtering. However, as the peak intensity of the solar wind implant is at a depth of only ~40 nm in the Genesis collectors, even with exceptional measures, the intrinsic limitations of ion beam mixing result in a sputtering region that changes with depth until steady-state is achieved; this transient region at least partially affects the solar wind depth profile when sputtering is initiated from the front-side of a collector surface.

Given these constraints, to obtain accurate depth profiles we adopt the method of sputtering from the backside of a collector target (backside depth profiling) with a low impact energy primary ion beam. This technique has been previously applied in the semiconductor industry for analysis of ultrashallow ion implants or impurities (e.g., Fujiyama et al., 2011; Jackman et al., 1990; Yeo et al., 2002; Yeo et al., 2003). We developed this technique further in our laboratory for the application to solar wind analysis.

In this contribution, we show that our backside depth profiling technique is capable of analyzing nearly complete depth distributions of many elements in the solar wind, even in the presence of high levels of surface contamination. We have successfully applied the method to the analysis of bulk solar wind with fluence as low as 2×10^{10} atoms cm^{-2} and, for some more abundant elements, to analysis of all three solar wind velocity regimes collected by Genesis (Reisenfeld et al., 2013). The regime collectors were only exposed to solar wind during specific conditions: slow (fluence-weighted mean proton speed: 384 km s^{-1}), fast (578 km s^{-1}) and coronal mass ejection events (CME) (452 km s^{-1}) that includes higher energetic ions (up to 1600 km s^{-1}). These collections have only about one third each of the fluence of the bulk solar wind sample (Reisenfeld et al., 2013) and are characterized by different depth distributions of the implanted solar wind.

In the following, we describe sample preparation, point out potential pitfalls, as well as generally explain the SIMS analytical conditions, standardization of measured signal, and data reduction procedures. Possible systematic errors are considered and evaluated. We show that these procedures allow us to obtain precise and accurate absolute fluences of the implanted solar wind in both bulk samples and regime-specific targets. The solar wind fluences of the analyzed elements as well as their implications on solar wind formation processes will be published elsewhere. Preliminary data are published in several abstracts (e.g. Heber et al., 2013; Heber et al., 2014).

2. Backside depth profiling

2.1 Sample preparation

Fragments of Float-Zone (FZ) silicon wafers with implanted solar wind, on the order of 8×8 mm^2, were cleaned at the Johnson Space Center curatorial laboratory by megasonically activated ultrapure water (5 min at 40°C) that efficiently removed particles ≥5 μm (Allton et al., 2007) followed by exposure to UV radiation in an ozone atmosphere (30 min) that removed the molecular film contamination deposited in space (Calaway et al., 2007). Final steps involved cleaning in a sequence of ultrasonic baths with the following solvents: xylene, acetone, methanol, and deionized water. Note that, due to the impact of the Genesis science canister, almost all wafers (originally 10 cm in diameter) fragmented into pieces of a few to low tens of mm in size and many contain scratches and other impact marks. Particular care was taken to choose only fragments where there were no raised defects on the surface (large welded particles or other debris) which would tilt the sample when mounted face down, and which also had a minimum of gouges or large pits in preparation for backside polishing (Fig. 1a).
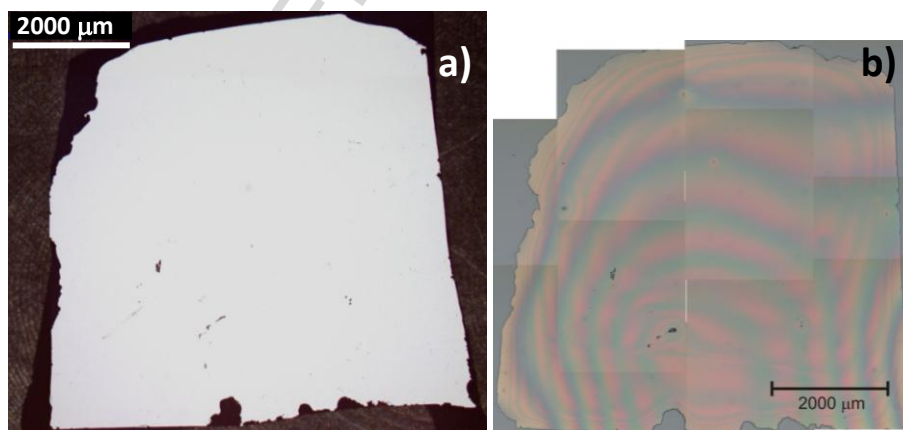
**Fig. 1.** Genesis Si fragment implanted with solar wind (sample 60869). a) shows the front side of the collector and b) the respective backside ground to ~1 μm thickness (the same scale is used for a and b). The dark marks are pits and gouges from the impact. Newton's rings in b) reflect the topography of sample. The flat area in the lower middle of the image is sufficient in size for many SIMS analyses.

2.2. Backside polishing

The backside samples presented in this work were prepared by the Evans Analytical Group (EAG), USA. The cleaned Si fragment (Fig. 1a) was glued upside down onto a Si substrate with epoxy (Fig. 2) and thinned mechanically. The polishing machine Allied High Tech MultiPrep™ was used and initial and intermediate polishing media were diamond lapping films of various grit sizes, the last one 0.5 µm grit size. The final polishing medium was a colloidal suspension of 0.02 µm silica. It is necessary to carefully monitor the thickness of the actual Genesis sample during the thinning, and not rely only on a measure relative to the surface of the substrate. When the Genesis spacecraft return canister crashed, particulates from the Utah soil as well as pulverized collectors and other impact debris from the spacecraft coated the collectors. Bits of other collectors (metallic, semiconductors) tended to weld to the surface and are impossible to completely remove. Moreover, particulates ~1 µm in size (and smaller) are difficult to remove due to strong adhesion, and therefore stick out from the front-side of the collector targets. They create a gap between the front-side of the collector and the surface of the Si substrate (filled with epoxy after mounting) that must be accounted for when thinning the silicon to a specific thickness. If the epoxy-filled gap caused by the presence of particulates is not considered, the sample will be thinned too much. In fact, both 400 nm samples (Table 1) that we prepared initially were intended to be thicker, but suffered from this inaccurate thickness measurement. As we will see below, the 400 nm thickness was less than ideal. We monitored the residual thickness of the collector using spectral reflectometry (Filmetrics F40 thin-film analyzer) during all following sample preparations. Over the course of our investigations multiple thinned Genesis Si collector samples were produced (Table 1) and the preparation procedure was optimized so that we were able to consistently produce samples with a reasonable large central, flat area (e.g., Fig. 1b) and an actual thickness within 100 nm of the desired target value.
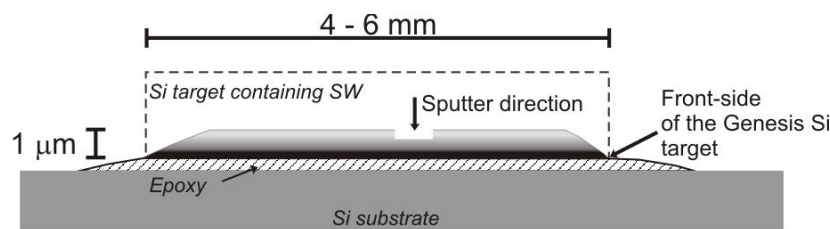
Fig. 2. Schematic edge-on view illustrating a backside sample. The gray-scale gradient in the Si fragment containing the solar wind mimics its concentration distribution as function of depth, as measured from the collector's rear surface. The dark strip adjacent to the epoxy represents the highest concentration, just beneath the surface that had been exposed to the solar wind.

We have found that for solar wind collectors the optimum thickness of a backside-polished sample is on the order of 800 nm. This allows sufficient space, about 200 nm, between the contamination of the rear surface (inevitably introduced during sample preparation) and the high energy tail of the solar wind implant that reaches to about 600 nm from the front-side for accurate background-level characterization. Somewhat thicker samples could also be utilized, however at the cost of increased total sputter time during analysis. Samples may become too thick at about >2 μm for certain analytical needs (e.g., the use of a large field aperture) as the raster pit narrows (i.e., the area of the bottom decreases) with depth.

In addition to careful control of the thickness, achieving an overall flat polish of the sample is also important. We monitored the surface shape of the 2.4 μm thin sample 30767 by using a Tencor P-20 stylus profilometer. The area of the flat surface in the center of this sample (but also of all other samples analyzed in this work) was on the order of 1 mm x 1 mm (see also Fig. 1). The flat area was exclusively used for analysis and a 1 mm^2 area was sufficient for ample SIMS analysis rasters. The slope of the ~2 mm-wide perimeter around the flat center area was assessed to be 20 nm over 100 μm in 30767. The smoothness of the polished backside was measured with a MicroXam interferometer and is about 0.1 nm (1σ standard deviation), or 0.6 nm between the minimum and maximum height over a

9

lateral distance of 20 µm, smooth enough to satisfy the depth resolution required in this study. An additional problem also arises because scratch marks are present on all samples due to impact debris (Fig. 1). "Deep" scratches and pits are easily avoided but scratches that do not penetrate to the polished backside are invisible at the start of sputtering but will lead to a premature "breakthrough" to the original sample surface and epoxy layer during depth-profiling (Fig. 3). Such problems can be avoided by careful sample documentation prior to gluing the sample face-side-down.
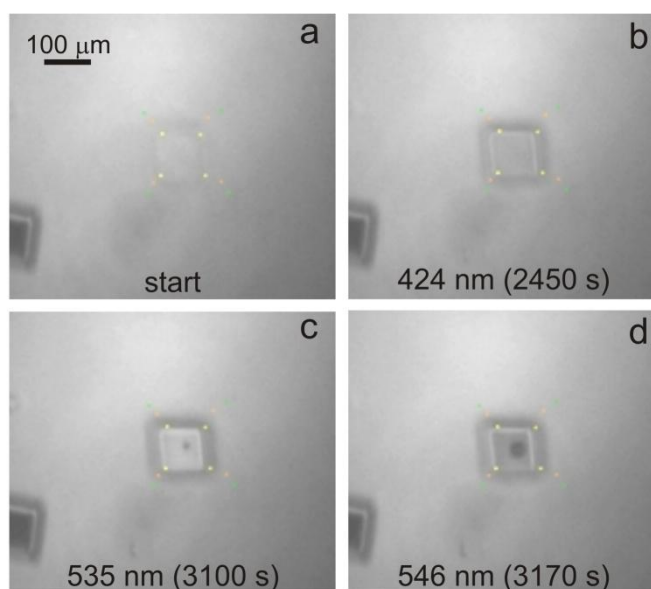
Fig. 3. SIMS analysis raster in the 600 nm thin backside sample 60514 (bulk solar wind) showing the effect of surface defects. (**a, b**): The area of the sputter pit and the sputter pit itself down to ~500 nm depth (from rear surface) were without marks. However, at ~530 nm (**c**) a hole opened that soon became larger to form a bubble and created a pathway to the surface and epoxy layers, from which contaminant ions overwhelmed the solar wind signal. The opening could be either due to a "hidden" scratch at the front-side, or due to some area not well glued to the substrate. Note, if the sample is thin (≤ 600 nm as in this case) the latter could cause frequent formation of bubbles (probably filled with evaporating epoxy) during sputtering as we observed also in the samples 60833, 41126b. The images here and in Fig. 4 are from screen captures of a video stream from a reflected light microscope and camera (the bright spots at the edges of the raster were on-screen fiducial marks).

Table 1

Genesis Silicon collectors prepared and analyzed by backside depth profiling.

NASA code	Solar wind regime	Thickness (nm)	Elements analyzed
60760	Bulk	400	Ca, Cr
60757	Bulk	360	C, N
30767	Bulk	2420	O, C
60968	Bulk	1080	Ca, Al, C, N, O
60514	Bulk	600	Na, Mg, Al
30768	Bulk	1130	Al, Cr
60796	Fast	640	Al, Ca, Na, Mg
41126a	CME	1250	Na, Mg
41126b	CME	510	Na, Mg, Al
41133	CME	920	Al, Ca
60833	Slow	520	Na, Mg, Al
60449	Slow	1030	Al, Ca

## 3. SIMS analytical conditions for backside depth profiling

Depth profiling analyses for C, N, and O were performed with the Cameca 7f-Geo at the California Institute of Technology and for Na, Mg, Al, Ca, and Cr mainly with the Cameca IMS-1270 at the University of California, Los Angeles. The IMS-1270 was chosen for analysis of the latter elements because high mass resolving power (m/Δm ~3000) is needed to separate the desired atomic ions from molecular ion interferences, and this can be achieved in that large-format instrument without sacrificing transmission. High instrumental sensitivity is needed to achieve good counting statistics as well as high peak to background ratios for low fluence ion implants, e.g., for Cr in bulk solar wind and many other elements in the solar wind regime targets. A summary of the chosen instrumental conditions is given in Table 2.

3.1. Primary ion beam conditions

The Caltech and UCLA CAMECA ion microscopes are normally employed in the analyses of geological materials in the dynamic SIMS mode, and as such, samples are biased at high potential (typically ± 10kV) to permit efficient extraction of emitted secondary ions with high lateral resolution (Slodzian, 1980). We used reduced impact energies for the primary ion beam, 5 keV for $^{133}Cs^+$ and 7 keV for O_2^+, to improve the depth resolution by reducing the primary ion range and thus the thickness of ion-beam-induced mixing layer. We took advantage of the conductive nature of Si metal to use O_2^+ as primary ion beam because it reduces the implantation depth and hence the initial nonequilibrium sputtering and also increases secondary ion signals compared to an O^- beam that is normally used for analysis of geological materials. These were the lowest impact energies we could achieve with reasonable focusing conditions as neither instrument is designed for ultralow impact energy sputtering. Furthermore, the angle of incidence of the primary beam is not independently adjustable in these instruments and the beam is deflected from the nominal 30° angle with respect to the sample normal as

12

it enters the acceleration space of the secondary ion extraction optics. The resulting angle and energy affect the implantation depth of the primary beam into the target; a calculation based on (Wilson et al., 1989) and the SRIM code (Stopping and Range of Ions in Matter, Ziegler, 2004) is given in Table 2 along with other sputtering parameters.

The primary beam was rastered over, in most cases, a 100 μm × 100 μm area and the current was adjusted between 12 nA and 18 nA to achieve sputter rates in the range between 0.1 nm s^{-1} and 0.25 nm s^{-1} (see equation 1 below for calculation). The primary beam current, monitored during (7f-Geo) or before and after the measurement (IMS-1270), as well as the count rate corresponding to a matrix element (Si, in our case) were constant within about 1% over few hours. This was a necessary condition as the depth of a backside profile was calculated from the sputter rate obtained from the measurements on standards made under the same analytical conditions. Furthermore, special care was taken to assure that the primary ion beams (either a focused Cs^+ beam or an aperture-illuminated O_2^+ beam) were tuned to attain a homogeneous density distribution on the sample surface so as to produce a flat-bottomed crater and thus a uniform break-through at the end of the backside depth profiling analysis (Fig. 4). The break-through was monitored optically during the measurement via the change in reflectivity as the beam penetrated through the fringes in Si to the epoxy layer (Fig. 4).
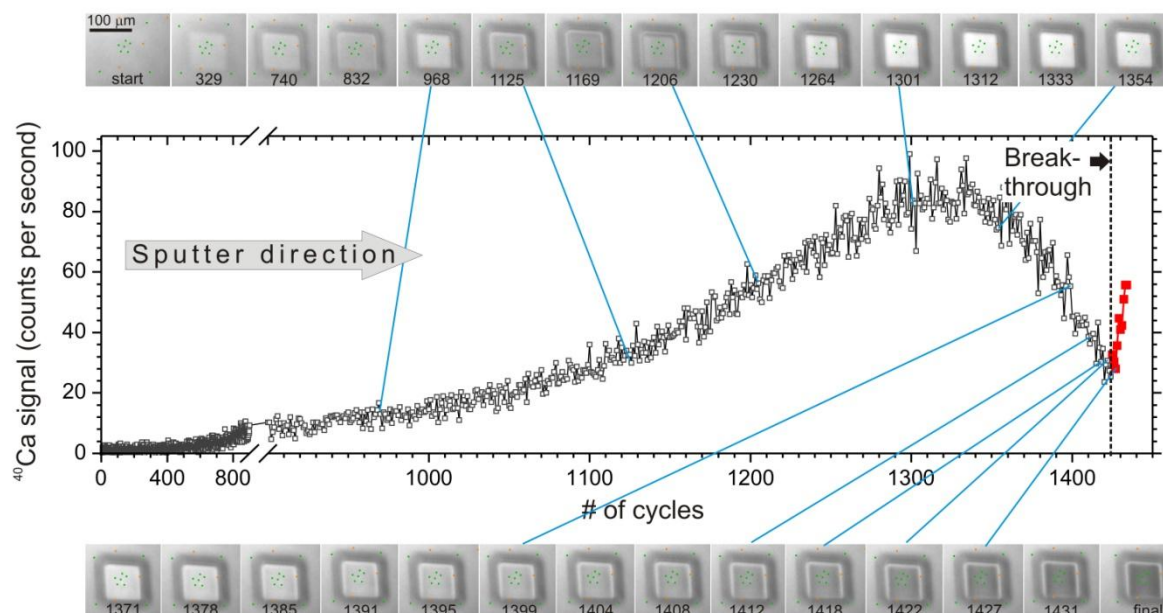
Fig. 4. Backside depth profile of solar wind $^{40}Ca^+$ (in counts per second, cps) measured in the fast solar wind regime (sample 60796) and plotted versus the number of cycles of this analysis. The photomicrographs are screen captures from the reflected light video camera taken during the analysis, the numbers representing the respective cycle the picture was taken (the spots in and around the raster were on-screen fiducial marks). The time interval between two cycles is 3.2 s corresponding to an erosion rate of 0.5 nm per cycle. The different gray-scales reflect the sputtering through the different levels of fringes (see Fig. 1) and were used to assess the flatness of the bottom of the sputtered crater. The vertical, dashed line indicates the break-through through the surface into the epoxy. This transition is characterized by an immediate and strong increase of the count rate due to contribution of contaminating ions to the solar wind signal. Those data, shown in solid squares here, were excluded from further evaluation.

3.2. Secondary ions

Secondary ions sputtered from the center of the crater were selected by use of a "field aperture" inserted into a secondary ion image plane in the mass spectrometer. This physically masks ions coming from outside the transmitted area and thus avoids crater wall contributions to the measured signal. The size of the field aperture (square, fully adjustable at the IMS-1270, round and fixed sizes at the 7f-Geo) was optimized at the beginning of an analytical session to make a compromise

between admitting only ions emanating from the flat crater bottom (as determined by using a MicroXam interferometer to measure a representative crater) and simultaneously maximizing the secondary ion signal and the duty cycle. For example, if the flat bottom of a 1 μm deep, (100×100) μm^2 O_2^+ sputter pit was on the order of ~(65×65) μm^2, the detected area was adjusted to about (45×45) μm^2. The raster size and the size of the field aperture were calibrated at the beginning of each analytical session and kept constant for the duration of that session. For the negative ion analyses (C, N, and O) the smallest field aperture had to be used resulting in a detected area with a diameter of only ~12 μm and, additionally, an electronic gate was used to further exclude ions from the outer 50 - 70% of the sputtered area. These measures were necessary to reduce the contribution of scattered ions of C, N, and O from surface contamination and vacuum deposition.

Table 2

SIMS analytical conditions.

	Analytical Sessions		
	Cameca 7f-Geo	Cameca 7f-Geo	Cameca IMS-1270
Primary ion beam	Cs^+	O_2^+	O_2^+
Primary / secondary accelerating voltages (kV)	+3 / -2	+13 / +6	+17 / +10
Impact Energy (keV)	5	7	7
Impact Angle (° relative to sample normal) (Cameca, 2004)	23	43	51
Nominal implantation depth (nm) (Wilson et al., 1989)	5.1	11.0	9.4
Nominal implantation depth (nm) (SRIM code)	7.9	9.6	8.8
Range of primary ion beam current (nA)	10 - 11	37 - 41	12 - 18
O_2 flood	No	Yes	Yes
Sample chamber pressure (mbar)	$(<1.3 - 2.1) \times 10^{-10}$	$(1.5 - 1.6) \times 10^{-5}$	1.5×10^{-5}
Liquid N_2 trap in sample chamber	yes	no	no
Range of sputter rates (nm s^{-1})	0.23 - 0.24	0.18 - 0.20	0.10 - 0.25
Nominal raster size (μm)	100 75 (2012)	100	95 and 100
"Projected" field aperture size (μm)	12 – 13 *(diameter)*	40 *(diameter)*	35 - 45 *(side length, quadratic)*

15

|			
Electronic gating (%)	session 1: 50% session 2: 70% (O,C), none (N)	none	none
Analyzed elements	C, N, O	Ca, Al	Na, Mg, Al, Ca, Cr
Mass resolving power (MRP = M/ΔM)	500	2600: Ca 1000: Al	2000 - 3000

3.3. Detection

Elements were analyzed by magnetic field peak switching using the axial electron multiplier (EM) for the implanted isotope and a Faraday cup (FC) for the matrix element (Si). Count rates were corrected for the effective deadtime, which is the intrinsic deadtime of the EM (44.3 ns for 7f-Geo, ~30 ns for IMS-1270) divided by the duty cycle, that was determined for each session. The duty cycle is the ratio of the gated secondary beam (rastered primary beam) to the full secondary beam (unrastered beam) or, for a well focused beam, the ratio of detected to rastered area (Wilson et al., 1989). The fluences of the elements in most of our reference implants and, even more so, of the solar wind samples, were low enough that the correction was insignificant or within the given uncertainties for the solar wind fluences. The effective deadtime of the positive ion measurements was on the order of 200 ns, corresponding to a maximum correction of less than 1% at the intensity peak of the reference implant. The effective deadtime of the negative ion measurements was on the order of 2000-3000 ns (owing to the very small detected area of a diameter of ~12 μm) and corresponds to a maximum deadtime correction of 0.6 - 3% at the intensity peak of the reference implant, depending on the element. Uncertainties in the determination of the duty cycle cause only a fraction of the applied correction and are thus negligible.

4. Sample analysis

4.1 General analytical conditions

Backside depth profiles of implanted solar wind were generally analyzed in three to four steps (Fig. 5). At first, a (125×125) μm^2 raster (step 1) removed the surface contamination of the backside sample until the measured intensity of the isotope of interest reached background level. This was followed by a (100×100) μm^2 raster for analysis (steps 2 to 4). During steps 1 and 2, both the isotope of interest and the matrix element were measured. During step 3 only the isotope of interest was measured to avoid loss of data due to the waiting times during switching of the magnetic field. Upon completion of step 3 the count rate of the matrix element Si was measured again on a nearby tuning spot in step 4. Each element presented here was measured separately, with the exception of Mg and Na (Fig. 6), to maximize the data coverage especially over the solar wind peak and down the portion of the profile closest to the collection surface, which is crucial for the fluence evaluation.
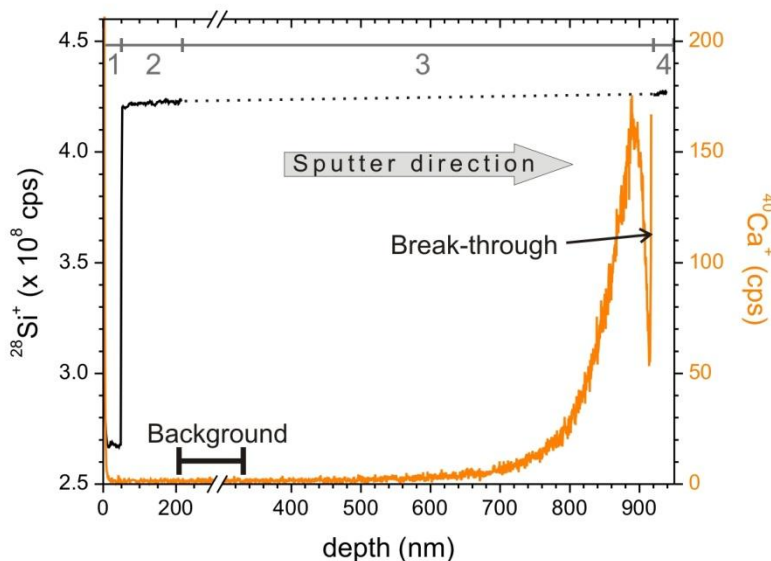
Fig. 5. Backside depth profile of solar wind $^{40}Ca^+$ (in counts per second, right ordinate) measured in the CME regime (41133). The numbers 1-4 (here and in Fig. 8) indicate the different analysis steps described in the text. The left ordinate represents the measured count rate of the matrix element Si^+ (shown in black). The lower Si^+ count rate in step 1 is due to the larger raster size (125 µm) and the resultant lower sputter rate. Note, Si was measured only in steps 1, 2, and 4 and was interpolated during step 3. The slight increase of Si over the entire analysis is due to a continuous, slight sputtering of the L4 and PBMF apertures by the primary O_2^+ beam, resulting in slightly higher primary ion current over the 1h 46 min of the analysis. The $^{40}Ca^+$ count rates between 220 nm - 330 nm represent the background. At 915 nm the primary beam hits the interface between the solar wind sample and the substrate characterized by a sudden and strong increase in the $^{40}Ca^+$ count rate.

Artificial ion implants with known, homogeneous fluences served as references and were routinely measured before and after each sample during positive ion analysis or several times per day during the negative ion analysis. From the reference implants (= standards) we obtained the Relative Sensitivity Factor (RSF; see below for explanation) and the sputter rate (see equation 1 below). The latter was used to determine the depth of the pits sputtered in the backside sample, a quantity required for calculating the implanted solar wind fluence. Note here an important complication of backside profiling: unlike pits resulting from conventional front-side analysis, it is generally not possible to measure the depth of a pit in a backside sample, as the sputtered area penetrates into the epoxy and below. Interferometers do not correctly interpret the different reflectivities of epoxy and Si; therefore, epoxy at the bottom of a pit in silicon can lead to artifacts and erroneous depths if an interferometer is used. A mechanical (stylus) profilometer is not a suitable solution either as the pit bottom (or the remains of it) is too fragile for the scanning diamond needle, in particular when holes into the epoxy are present (which is the case for most of the analyses). Hence, in order to obtain accurate and precise elemental fluences from backside depth profiling analysis, it is essential to measure the sputter rate as close in time as possible before and after the sample by using standard materials of the same matrix. Those are generally sputtered from the front-side and their pit depths are easily measured either by interferometry or with a profilometer.

18

All analyses (standard and sample) were done under identical conditions per given session. Care was taken to reduce instrumental background to acceptable levels. For volatile elements, this involves maintenance of ultra-high vacuum conditions in the sample analysis chamber and, in particular the reduction of the residual partial pressure of water. Another source of instrumental background of all elements at a low level is due to unintended sputtering of instrument surfaces in the primary ion column and the sample chamber. Particularly important because of its close proximity to the sample analysis area is tertiary sputtering of the immersion lens extraction plate leading to a release of matter from previous analyses (e.g., of aluminum due to sputtering of an Al-sample holder, or oxygen from sputtering silicates and epoxy). An effective strategy to reduce this background contribution is to cover up the contamination with a pure element. This was achieved by intense (500 μm raster: Cs^+ 150 nA, O_2^+ 1 μA) overnight sputtering of a pure Si target prior to analysis of the Genesis samples. For some refractory contaminant elements, this procedure was critical to obtaining accurate solar wind abundances, e.g. the Al background was reduced by an order of magnitude by this "sputter cleaning". Several specific analytical procedures were applied, tailored to the conditions required by the positive or negative ion analysis of solar wind.

4.2. Positive ion (Mg, Na, Ca, Al, Cr) analysis

A gaseous oxygen bleed into the sample chamber reduced initial nonequilibrium sputtering and increased the secondary ion signals by a factor of about three for all analyzed elements (with the exception of Na). The sensitivity of Na had been higher without the O_2 bleed, but as Na and Mg were analyzed together (see below) and the Na signal was still sufficiently high, the lower Na sensitivity was accepted for the sake of Mg. The secondary signal was constant for the range of O_2 pressures of (0.9 - 2.0) $\times 10^{-5}$ mbar; we adopted (1.3 - 1.6) $\times 10^{-5}$ mbar for all analyses.

We applied sufficient mass resolving power (MRP) to remove all significant molecular ion interferences from the signal of interest. The MRP was 2000 for the ^{24}Mg-Na analysis (that resolved the

NaH interference on mass 24) and 3000 for Al ([26]MgH resolved), [40]Ca ([28]Si[12]C and [24]Mg[16]O resolved, a contribution of [39]KH was tested and considered negligible), and [52]Cr ([28]Si[24]Mg resolved, a contribution of [51]VH is unlikely in our samples based on the factor of 40 lower [51]V solar abundance compared to [52]Cr).

During positive ion analysis all solar wind sample measurements were bracketed by standard implants measured alternately in the same 7 mm center-hole sample holder. We did not observe any memory effects that could have been caused by the higher fluences of standard implants. The strict sample-standard bracketing was particularly important for part of this work that required relatively high precision: favorable analytical conditions for some positive ions (high sensitivity, low background, etc.) permitted their analysis in the solar wind regime samples, for which we expected differences in the relative fluences (e.g., the Al/Ca elemental ratio) on the order of only several to some 10 percent; thus a close control on the instrumental conditions, the RSF and the sputter rate was mandatory.

In contrast to Ca, Al, and Cr, both Na and Mg were analyzed together in two steps, starting with a 110 μm raster to remove surface contamination, followed by a 95 μm raster for the solar wind implant analysis (Fig. 6). Also, for these analyses the matrix element Si was detected throughout the solar wind analysis. This procedure was performed mainly to increase our solar wind data output during the session and because we knew, based on our Mg isotope measurements (Heber et al., 2012b), that complete solar wind profiles can be obtained for Mg despite peak jumping. The standard we used was likewise implanted with isotopes of both elements ([25]Mg, [23]Na). Several interesting features can be seen in the depth profiles of Mg and Na, as shown for example in Fig. 6 for a fast solar wind sample. At the solar wind implant peak, the Si^+ count rate decreases by maximum 0.6% compared to its general trend, with the shape of this part of the curve mimicking the H implant peak in reverse. At this point we do not know whether this slightly reduced Si count rate is due to dilution of the Si substrate due to the high concentration of implanted solar wind hydrogen in this region (peak concentration is 5×10^{-3} proton per Si atom for the H fluence of 6.4×10^{15} cm^{-2} in this sample) or due to a matrix effect (i.e., change in

20

ionization rate due to the different chemistry). The change in the Si signal that is almost exactly reflective of the change in H concentration, 0.6% versus 0.5%, though argues against a significant matrix effect. In any case, Mg and Na fluences were calculated relative to Si with the assumption that whatever the reason is it affects matrix and trace element to a similar extent. Also, the overall effect on the solar wind fluences of the elements considered here is less than a percent and thus well within uncertainties obtained with our analytical procedure. The break-through of Na is always earlier than that of Mg, about 8 nm in this fast solar wind sample, and more vigorous (at the break-through the count rate of Na is ~1.5 orders of magnitude higher than Mg). We speculate that either a Na-rich thin film remained on the surface of the target despite extensive cleaning or, more likely, Na is a trace constituent in the epoxy we used for sample preparation. Primary ions penetrating beyond the Genesis target may backward-garden Na atoms from the epoxy or the thin film that finally dominate the secondary signal (Fig. 7; see also section 4.3). Also the instrumental Na background is always higher than that of Mg: the background to peak intensity is 2-16% for Na, depending on solar wind fluence of a sample, compared to only 0.07-0.5% for Mg.
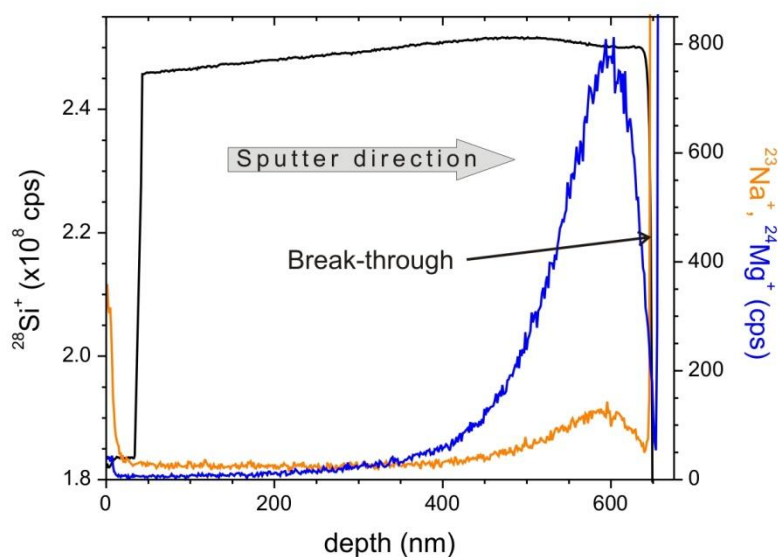
Fig. 6. Backside depth profile of solar wind ^{23}Na$^+$ (orange, lower count rates) and ^{24}Mg$^+$ (blue, higher count rates) (right ordinate) measured in the fast solar wind regime sample (60769). The left ordinate represents the measured count rate of the matrix element Si$^+$ (shown in black). The lower Si$^+$ count rate up to 50 nm (step 1) is due to the larger raster size (110 µm). Here, Si was detected over the entire course of the solar wind analysis. The slight increase of Si during the analysis is due to a continuous, slight sputtering of the L4 and PBMF apertures, similar to that shown in Fig. 5. The drop of Si at the end of the profile (~650 nm) indicates the primary beam tapping the interface epoxy. Fig. 7 shows an expanded scale of the implant peak region and the break-through.

We test the possibility of whether an increased diffusive mobility of Na could be the cause for the earlier break-through by comparing the widths of the measured implant peaks of Na and Mg. Figure 7 shows the region of the implant peak and the break-through in more detail exemplarily for two analyses. We chose depth profiles in a fast solar wind sample (same as in Fig. 6), because its Na profile is most complete due to the deeper implantation depth, and in a bulk solar wind sample, because of the larger fluence and thus less data scatter. In both examples, but also in all other analyses (not shown), the break-through of Na is earlier than Mg, by 8 to 10 nm, as mentioned previously. Also, Na is implanted about 2 - 3 nm deeper than Mg, an observation made for all analyses in all solar wind regimes. The fact that Na is implanted deeper than Mg is predicted by simulations by SRIM, although SRIM predicts only about half the difference between Na and Mg (~1.5 nm). More importantly, note that the peak width is similar in both Mg and Na implant profiles. If Na had diffused during solar wind collection, there should have been peak broadening: based on our data we can safely exclude a recognizable mobility of Na in silicon collectors of all solar wind regimes of the Genesis spacecraft.
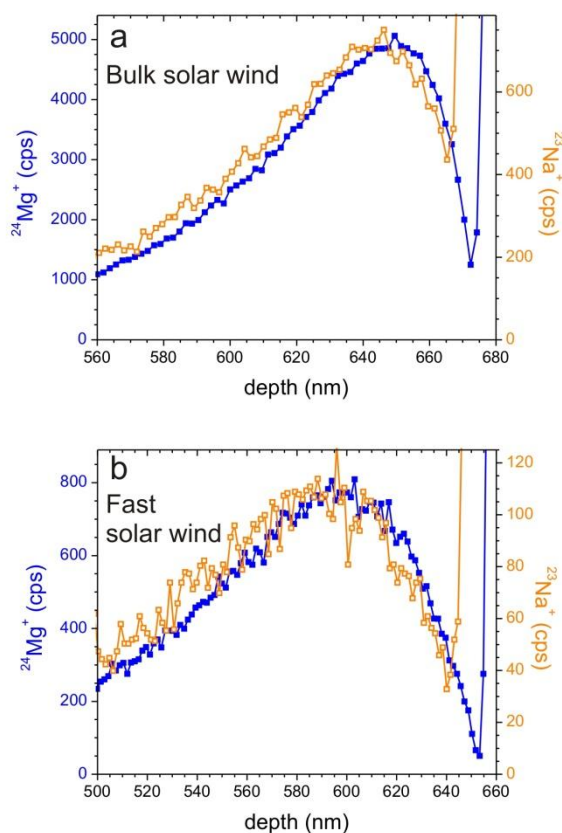
Fig. 7. Sections of measured and background corrected depth profiles of Na and Mg depicting in more detail the region of the implant peak and the break-through. A) is a bulk (60514) and b) a fast solar wind profile (the same as in Fig. 6). The ordinate represent the measured count rates of $^{24}Mg^+$ (left, solid squares) and $^{23}Na^+$ (right, open squares). Clearly visible is the earlier break-through as well as the slightly deeper implantation depth of Na compared to Mg.

4.3. Negative ion (C, N, O) analysis

Surface contamination and an elevated instrumental background complicates, and can even inhibit, the analysis of low concentrations of C, N, and O, as present in the solar wind. Therefore, the following measures were applied to reduce the background to allow us to measure almost complete solar wind profiles of these elements in Genesis collectors that did not concentrate the solar wind. (Note, that Marty et al. (2011), Marty et al. (2010) and McKeegan et al. (2011) analyzed a higher fluence

sample from the Genesis solar wind Concentrator (Wiens et al., 2013) to determine the N and O isotopic composition of solar wind.) i) The primary and the secondary column and the sample chamber of the 7f-Geo were baked at 120°C for about 48 h before the start of the sessions. ii) The sample chamber was additionally pumped with the Ti sublimation pump overnight. iii) We strictly avoided any sample change during the period of sample analysis of a few days (the valve to the airlock chamber remained closed). iv) An ultra-pure float-zone Si wafer was intensively sputtered overnight to cover the immersion lens extraction plate. v) Finally, a liquid nitrogen cold trap fixed residual water in the sample chamber vacuum. With these measures we were able to reduce the pressure in the sample chamber to 2.1×10^{-10} to $<1.3 \times 10^{-10}$ mbar for these analyses. However, although the exposure of epoxy was minimized and a low-vapor pressure epoxy was used, it nevertheless still contributed to the residual vacuum.

The samples and standards were placed in a 4-hole Cameca sample holder (instead of our usual single-central hole mount) as changing samples would have ruined our low instrumental background. Before or after the period of sample analysis, we carried out extensive standard measurements to assess the reproducibility with regard to quantifications of fluences measured at different positions in this holder. Deviations between the different positions were on the order of 0 to 6.6% and measured data were corrected accordingly.

To maximize sensitivity, we utilized low MRP during the analysis (M/ΔM = 500). Interferences on ^{12}C and ^{16}O in the solar wind sample are insignificant; the same is true for ^{13}C and ^{18}O in the reference implants, as the fluences of these normally minor isotopes exceed those of the ^{12}C and ^{16}O isotopes by large amounts. Nitrogen was analyzed as the ^{28}Si^{14}N$^-$ molecule, as nitrogen does not form negative atomic ions. Due to the low MRP the measured signal on mass 42 in solar wind analyses had to be corrected for the contribution of interfering ^{30}Si^{12}C$^-$ by 3.6%. The value was calculated based on ^{28}Si^{12}C$^-$ measured concurrently in a solar wind sample in both sessions. A possible contribution of the ^{12}C^{14}N^{16}O$^-$ molecule was found to be negligible.

C, N, and O backside depth profiles were measured in three steps in the solar wind sample, without step 4 (see section 4.1.), a procedure justified because of the great stability of the 7f-Geo during our sessions; e.g., the Si^- count rate varied much less than 1% over an 80 min run. Also, the uncertainty of the negative ion fluence measurements in the solar wind samples is somewhat larger due to lower count rates and less complete depth profiles compared to those of the positive ions (e.g., compare Figs. 8 and 9 with 5 and 6).

All C and O depth profiles obtained from the solar wind samples resemble the one shown in Fig. 8b for O, with the break-through always at the implant peak. For N, the depth profiles may extend slightly beyond the peak, as shown in Fig. 8a. The primary reason for this poorer separation of the solar wind signal from the contamination, relative to that achieved for the positive ions, is the high abundance of these elements on surfaces and in the epoxy used to glue the solar wind target onto the substrate. Thus, a few primary ions penetrating into and backward-gardening C, O, and N atoms from the surface layers and the epoxy interface, respectively, are sufficient that the secondary signal is dominated by these contaminants. In some sense, this is unavoidable for these volatiles opposite to the positive ions measured here - even by backside profiling: the uppermost 3 - 5 nm of the metallic Si wafer consists of a native Si oxide (SiO_2) layer (Calaway et al., 2009). Furthermore, in many cases, a carbon- and oxygen-rich, UV-polymerized thin film, <5 nm in thickness and deposited in space, is present (Allton et al., 2006). This layer was partially removed by exposure to UV radiation in an ozone atmosphere. Finally, C, O, and N are the main constituents of epoxy.

Attempts were made to cover the front-side of a solar wind bearing Si wafer with a 20 nm layer of Si by e-beam deposition before attaching it to the substrate. We hypothesized that this layer would delay primary ions sputtering into the epoxy, possibly leading to more complete profiles of solar wind N and other elements. However, the shear-strength of the bond between the Si wafer and the e-beam deposited Si was too low, so that the coating failed mechanically during the backside thinning process.
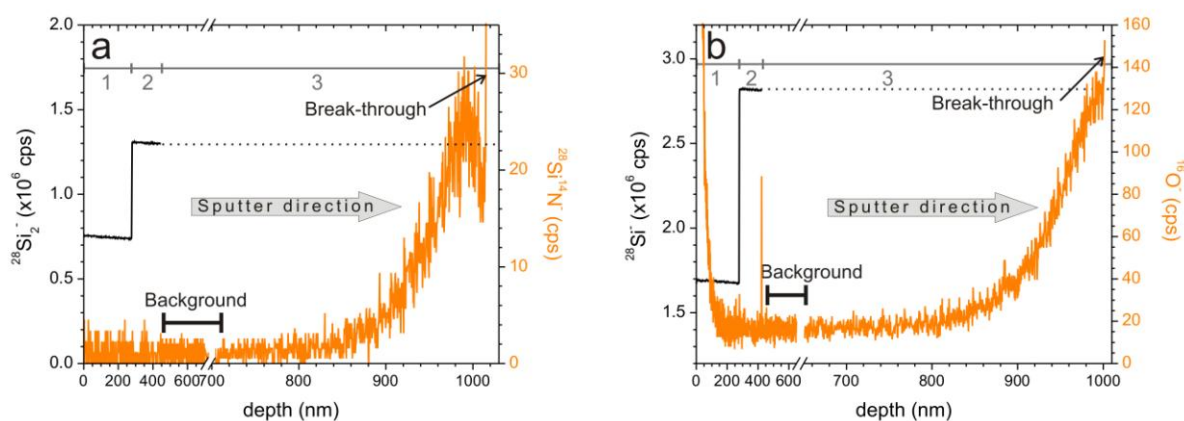
Fig. 8. **a**) Typical backside depth profiles of nitrogen ($^{28}Si^{14}N^-$) and **b**), oxygen ($^{16}O^-$) measured in the bulk solar wind sample (60968) (right ordinates, respectively). Depth profiles of $^{12}C^-$ resemble the one shown for $^{16}O^-$. The left ordinate represents the measured count rate of the matrix element Si^- or Si_2^- for O and N profiles (shown in black), respectively. The lower Si^- count rate up to 300 nm (step 1) is due to the larger raster size (100 μm in this session compared to 75 μm for the subsequent analysis).

4.4. Depth measurement

For each analysis in our standard implants, the depth of the pits was measured by using one of two interferometers, MicroXam Surface Mapping Microscope and Zygo optical surface profiler. Note, measurements of the pit depths of the backside-thinned samples were tried, but often resulted in meaningless data (see section 4.1.). Multiple measurements on both instruments resulted in consistent depths with variations of less than 0.5%. The accuracy of the depth measurement was regularly verified with a NIST standard (88 nm) that was reproduced to ±2 nm. Considering that the majority of the pit depths were on the order of 400 nm to 1 μm, the uncertainty due to depth measurement is very small, less than 1%.

5. Data reduction in backside depth profiles

The Si-normalized relative sensitivity factor, RSF, of each element analyzed in this work was determined from respective reference implants measured prior to and after the sample profile. In SIMS depth profiling, by convention the RSF is a conversion factor from secondary ion intensity to atom density (see section 3.1 in Wilson et al., 1989):

$$d_i = (n_i / n_{Si}) \times RSF \qquad (1),$$

where d_i represents the atom density and n_i the ion intensity in counts per second of the element of interest, and n_{Si} the ion intensity in counts per second of the matrix element (silicon in this case). The unit of the RSF is atom cm^{-3} and the RSF is specific for a given matrix (Si in this case). From ion implants, RSFs are calculated by dividing the nominal fluence of the reference implant (F_i, unit atoms cm^{-2}) by the ratio of the measured intensities of the element of interest to the matrix element (n_i / n_{Si}) integrated over the total depth (x) of the measured depth profile according to:

$$F_i = RSF \times \int (n_i / n_{Si}) \, dx \qquad (2).$$

From the total pit depth (x) and the total sputter time (t) we obtained the sputter rate (S) for each analysis of the reference implant:

$$S = x/t \qquad (3)$$

Table 3 lists the RSF's for all elements measured in this work. With the RSF and S, the unknown solar wind fluence of an element (F_i) in the sample can be calculated from its depth profile according to equation 2 with the integral of the measured (n_i / n_{Si}) taken over the entire depth of the implanted solar wind assuming S to be constant.

The detected signal of the isotope of interest was corrected for background contribution and counting system effective deadtime. No corrections were made for instrumental mass fractionation between the isotopes in the standard (the minor isotope in most cases) and the sample (always the major isotope) as such effects are minor, generally in the permil range for heavier elements. Even for C, where instrumental mass fractionation effects are in the few percent range, this correction is not necessary as it is smaller than the typical uncertainty of the final C fluence determinations. Final fluences were corrected for backscatter loss at implantation into silicon; respective correction factors were obtained by the SRIM code using measured solar wind velocities (see below) and range between 0.005% (^{52}Cr) and maximal 2% (^{12}C).

Table 3

Relative sensitivity factors for elements measured in this work.

Element	Mean RSF ($\times 10^{22}$ atoms cm^{-3})	n	# of sessions	
C	4.7±0.6	51	3	7f-Geo, 5 keV Cs$^+$
O	3.5±0.7	67	3	
N	0.81±0.04*	28	3	7f-Geo, 5 keV and 19 keV Cs$^+$
Na	0.502±0.065	12	2	
Mg	1.01±0.08	16	2	IMS-1270, 7 keV O$_2^+$
Al	1.43±0.02	22	2	
Ca	0.966±0.006	14	1	
Cr	2.50±0.09	14	2	IMS-1270, 7 keV O$_2^+$
Ni	2.66±0.15	13	2	7f-Geo, 6 keV O$_2^+$

RSFs are with respect to the matrix element Si (*Si$_2$ for N). They are related to one preferred reference implant per element (see Table 4 for more information), measured during several sessions and in some cases on both SIMS instruments.
Mean RSFs were calculated from average RSF of each session, the given uncertainty represents the variability of the RSFs between the sessions (1 σ standard deviation). n is the total number of analyses.

For profiles as shallow and element concentrations as low as in the solar wind ion implants, our backside profiles are not hundred percent complete. Accordingly, we face some additional complexity in

28

data reduction to account for the missing portion of the profile. For elements like O the break-through into the SiO_2 layer and the epoxy occurred near the peak of the implant profile (Figs. 8, 9), whereas other elements resulted in nearly complete profiles (e.g., Mg) and some elements were in-between (e.g., Na). At break-through the solar wind signal was immediately overwhelmed by ions from surface contamination and epoxy, at which point the measurement was stopped. Thus, the total fluence of an isotope (F_T) in the solar wind implant had to be calculated by adding the "lower limit fluence" = F_{LL} and the "estimated fluence" = F_E from the very near-surface portion of the profile that was unrecovered by the backside depth profile. The lower limit, F_{LL}, is easily obtained by integration of all measured data of the depth profile up to the point of break-through according to Equation 2. To calculate F_E, the "missing" part of the depth profile, we must extrapolate a measured profile to the original surface of the sample using a model depth profile shape. The accuracy of the models can be assessed by the level of agreement of the theoretical curves with the backside depth-profiling data for those elements, like Mg, where a nearly complete profile was recovered, i.e., where the missing part of the depth profile was minor. Refinements to the curve-fitting are discussed below for specific cases.

Generally, for the curve fitting, we must first estimate D_E, defined as the distance from the last "good" measured point before break-through to the original surface of the solar wind collector (Figs. 9 and 10). This estimate is only reasonably sound if the measured profile reaches at least to the peak of the solar wind implant, which is the case for all profiles investigated here, even though marginal for oxygen and carbon. The general functional form is approximately known from a theoretical model utilizing the code SRIM (Ziegler, 2004). The specific parameters for the solar wind implant model is constrained for each element in the Genesis Si collectors by the solar wind speed distributions measured with the Advanced Composition Explorer (ACE) spacecraft during the time of Genesis operation (Reisenfeld et al., 2013). Empirical fits to measured depth profiles have also been used.

First, we made a direct comparison of the measured profiles against theoretical curves modeled by the SRIM code, with the SRIM curves adjusted only to match the data at the peak intensity (Fig. 9). Measured and modeled profiles resemble each other, and the model curves reproduce characteristic features of the measured profiles for the given solar wind parameters, e.g., the relative widths of the implant peaks of different solar wind regimes. However, to estimate F_E by simply integrating the portion of the SRIM curve from D_E (D_E being estimated in this case as the distance to the surface as indicated by the SRIM curve) is too uncertain, due to significant deviations of the measured data from the SRIM curves, which is true for all elements and solar wind regimes analyzed in this work (examples are given in Fig. 9). The SRIM curves are all more narrow and the measured depth profiles are slightly skewed relative to SRIM. This is particularly visible for the positive ion depth profiles that have much higher count rates and lower data scatter. The source of the disagreement could be either analytical, e.g., some profile smearing due to knock-on of ions during analysis, or due to the fact that SRIM may not perfectly simulate the implantation of solar wind, e.g., crystal structures (and hence ion channeling) are not accounted for in this code. Especially for the positive ion depth profiles, D_E and thus F_E would be overestimated if SRIM curves were used to define the "depth" of the original surface of the sample. This is illustrated exemplarily by Ca in Fig. 9f. Nevertheless, the overall integrals obtained from our measurements agree with the model expectations to some tolerance (the fluences obtained by integration of adjusted SRIM curves differ by a few to at most 15 percent from our final fluences obtained from measured data and respective fitting procedure, see below).
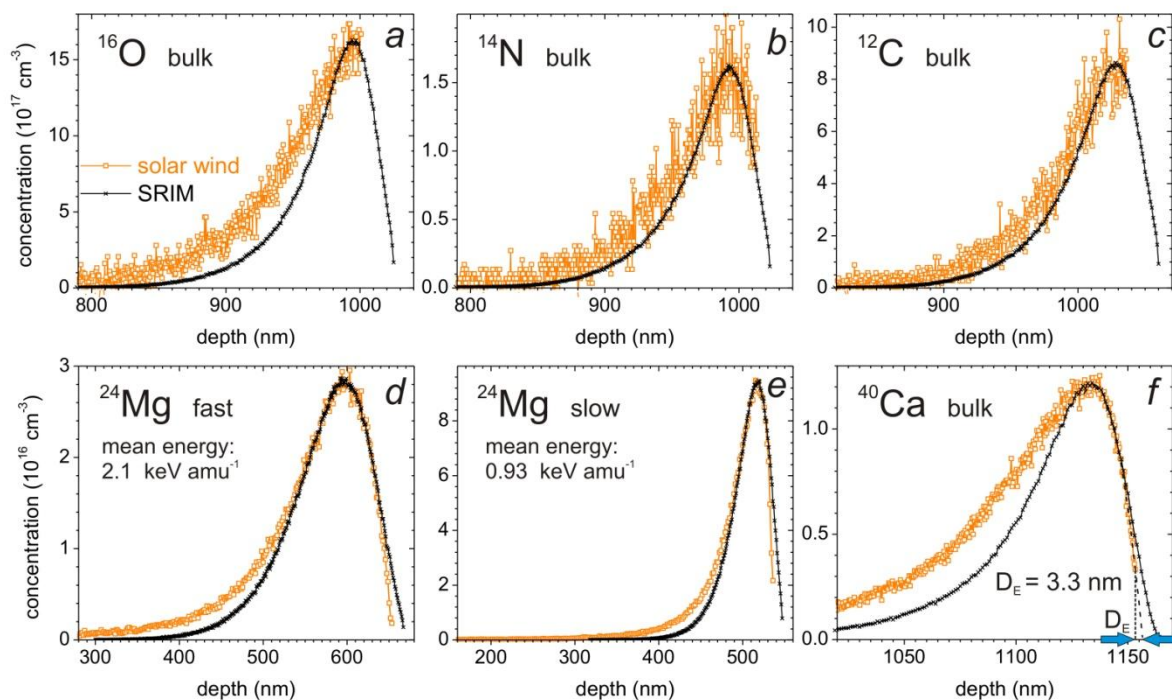
Fig. 9. Atomic concentration vs. the sputter depth for elements measured by backside depth profiling (orange, open squares) in comparison to the respective SRIM model curves (black line with crosses) that were adjusted in height and position relative to measured data. The sputter depth was obtained from S of the adjacent standard measurements (equation 3). Sputter direction is from the left. Measured data are plotted up to the point of break-through. **C, N, O (a-c):** The section of the abscissa is 250 nm in all three profiles. Due to the low count rate the measured profiles show a considerable scatter in the data; however, because of the large number of measurements, the counting statistics errors for a given profile are relatively low (e.g., ~1% for N). **Positive ions (d-f):** ^{24}Mg in fast and slow, as well as ^{40}Ca in bulk solar wind are shown exemplarily representing different implant energies. The measured profiles are virtually complete and the data scatter much less. None of the measured curves entirely agrees with their respective SRIM curves. In **panel f** in addition to the measured data and the SRIM curve we plotted the quadratic polynomial (dashed line) that was used to extrapolate to D_E (indicated by the two arrows, see also caption of Fig. 10) from the last measured data point (represented by the vertical dotted line). If the "depth" of the original surface was instead defined with the SRIM curve, it is obvious that D_E and thus F_E would be overestimated here and in all other positive ion depth profiles. Additionally, the comparison between the slow and fast solar wind ^{24}Mg depth profiles (panels **d** and **e**: both abscissae are 400 nm) clearly illustrates the much more shallow implant, i.e. close to the surface, and the more narrow ion distribution of

the low compared to the higher energy implant: the mean energy of the slow solar wind is 0.93 keV amu^{-1} and of the fast solar wind 2.1 keV amu^{-1}.

The most complete backside depth profiles were obtained for Mg, with D_E only being about 3 to 5 nm beyond the last measured point, whereas the least complete depth profiles were obtained for C and O, resulting in D_E on average of 23 nm (see O as example in Fig. 10f) . Generally, D_E was small for the majority of the depth profiles we obtained for positive ions, ≤ 10 nm (Figs. 9, 10), indicating that the backside profiling and sample preparation methods worked exceedingly well in these cases.

Measured depth profiles are well fitted by an asymmetric power function (Asym2sig in Origin®, Equation 4)

$$y = y_0 + A \cdot \frac{1}{1+e^{-\frac{x-x_c+w_1/2}{w_2}}} \cdot \left(1 - \frac{1}{1+e^{-\frac{x-x_c-w_1/2}{w_3}}} \right)$$

(4)

but the extrapolation asymptotically diverges at the surface, thus this function is not suitable to calculate F_E (see Fig 10 a-e). Note, we selected this function to describe the measured depth profiles and did not intend to use it to model ion implantation in targets. Instead, we found from investigating the nearly complete Mg depth profiles (obtained for all solar wind regimes), that a quadratic polynomial fits the measured data very well from the peak region all the way down the front-side of the profile essentially to the sample surface (Fig. 10a). Therefore, we employed this approach for all profiles which contain measured data that go past the solar wind implant peak and about one third of the distance down the front-side of the profile before break-through to the sample surface (see Fig 10a-c for examples). Thirty of our 39 measured positive ion backside depth profiles were treated this way to

32

obtain the integral F_E. A special case is represented by Na that was measured together with Mg. Despite sodium's earlier break-through by a few nm compared to Mg and, consequently, less complete profiles, the data were reliably fitted by the quadratic polynomial because the distance to real surface was set by Mg (Fig. 10, cf. panels a and d).

In nine of the positive ion depth profiles and all negative ion profiles, data coverage down the front-side of the profile was insufficient for application of this procedure. In such cases, to obtain F_E we utilized a more complete profile of the same element (when available) or, if necessary, another element from the same solar wind regime to obtain the fitting parameters (e.g., the shape of the Mg fit was used to extrapolate the Ca profile in Fig. 10e and the O profile in 10f). This strategy works because depth distributions of different elements implanted with the same energy distribution, i.e. from the same solar wind regime, are very similar; in particular, SRIM simulations show that the front-side profiles and the peak depths are virtually identical in these circumstances. In the example of ^{16}O (Fig. 10f), the extrapolated fluence calculated from the adjusted and fitted Mg profile amounts to 15% of F_T (with D_E = 22 nm) compared to the one of the almost complete depth profile of ^{24}Mg in example (Fig. 10a) where F_E corresponds to 1.1 % of F_T (with D_E =5 nm).
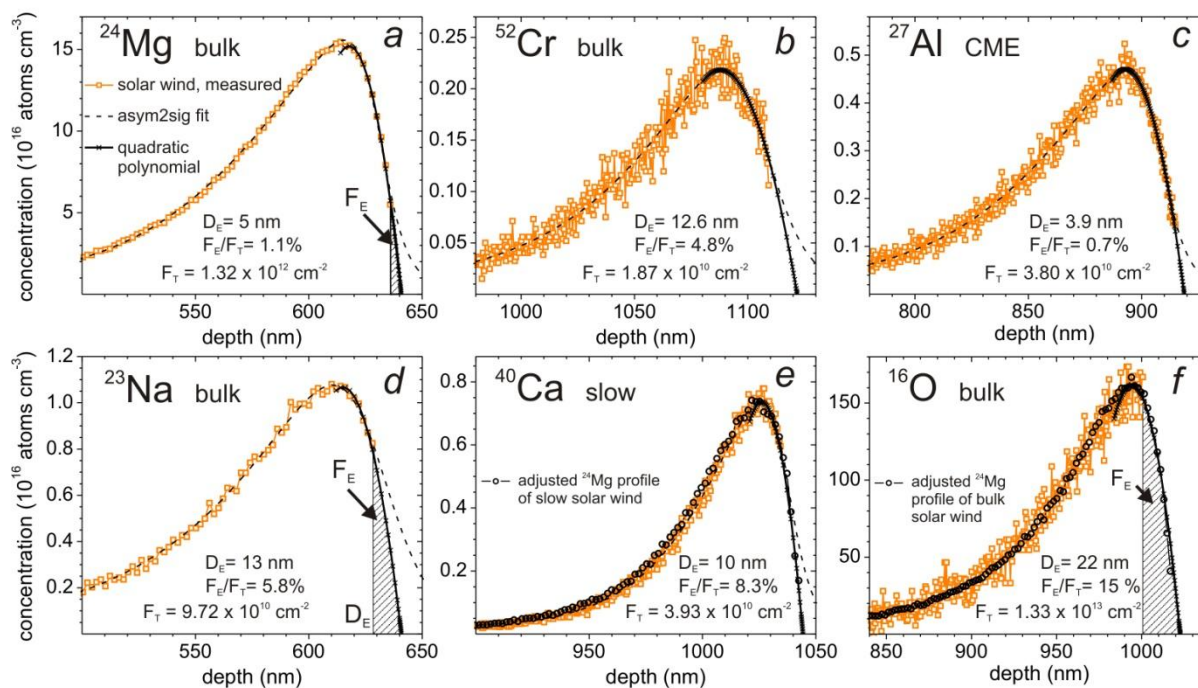
Fig. 10. Atomic concentration vs. the sputter depth for some elements measured by backside depth profiling. Measured data (orange, open squares) and respective fits (see legend in panel **a**) used to extrapolate to the real target surface at depth D_E are shown. F_E is the fluence (integral) between the last measured data point and D_E and is exemplarily shown in panels a, d, and f. In all panels the abscissa represents 150 nm near the original sample surface, except in panel **f** which has an extended depth scale (200 nm). The largest part of the depth profiles are well described by an asymmetric power function (black dashed line). However, to extrapolate to the original sample surface a quadratic polynomial was used (black solid line with crosses). In panel **d** D_E for the Na profile was determined from D_E of the respective Mg profile (panel a for this example), as both elements were measured together (see text). Panels **e** and **f** present examples of profiles with no or only few data at the front-side. In such cases, a Mg profile was adjusted to the measured data (in height and position) to allow extrapolation to the real surface. F_T, and D_E are given for the examples shown. F_E/F_T represents the magnitude of the surface correction to the total fluence, which is at most 15%.

6. Standardization and absolute calibration of the fluences of the reference implants

Sample fluences were calibrated against reference implants via the relative sensitivity factor (RSF), see section 5. The reference implants were produced based on the following criteria: the isotope fluence was chosen to be high enough to result in a secondary ion signal well above background but low enough to be measured on the electron multiplier with, if possible, only insignificant or low deadtime corrections. The use of a minor isotope of the element of interest increased the range of possible fluences to comply with these requirements. The implant energy was adjusted to sufficiently separate the reference implant from the surface contamination and non-equilibrium sputtering region, but at the same time to be shallow enough to allow extraction of 99 to 99.9% of the implanted ions in a reasonable time frame (< 2 hours). Fluences of the positive ion reference implants were on the order of 10^{13} ions cm^{-2} implanted with 1 to 5 keV amu^{-1} (Table 4). Negative ion reference standards were implanted with $(0.2 - 1) \times 10^{15}$ ions cm^{-2} in the range of 1 to 7 keV amu^{-1}. In general, we regard the energies of ≤ 1 keV amu^{-1} as too low using the analytical conditions presented in this work. Nonequilibrium sputtering and surface contamination may affect the first part of the depth profiles for lower range implants, which would require corrections that could affect the accuracy of the derived sensitivity factors.

Over the course of our investigations we utilized several reference implants per element produced by different implantation facilities. Table 4 gives an overview of the analyzed reference implants, their nominal fluences, and implantation energies. Our cross-calibration survey (Table 4) showed that nominal fluences of different implants often deviate by ~10%. There are many contributing factors for these variations. For example, the low mass resolving power, corresponding to only 0.5 amu in many ion implanters, in connection with low vacuum conditions ($\sim 10^{-6}$ mbar) could possibly lead to co-implantation of interfering molecules and isotopes (and thus an incorrect measurement of the fluence of the isotope of interest). In some cases, the total integrated current could be off by some

systematic amount; however, in our case, this is unlikely as the operators from two implant facilities (A and B, Table 4) assured us that their systems had been recently calibrated. Any errors in the fluences of the standards propagate directly into the errors of the RSF and thus can lead to inaccuracies in the fluences obtained for a sample. Therefore, we took several steps, tailored to each element, to absolutely calibrate the reference implants.

The fluence of the ^{25}Mg reference implant was calibrated relative to the Mg concentration in the NIST 617 glass (Eggins and Shelley, 2002; Reed, 1992), based on a method described by Leta and Morrison (1980). Thereby, ^{25}Mg was implanted simultaneously in a set of different targets, including NIST 617 and a float-zone Si wafer that would become the primary standard for depth profiling analysis as described above. Based on the known Mg concentration in the NIST glass (the Mg concentration was newly determined by Burnett et al. (2014, in press)), the RSF of ^{24}Mg was determined in the glass. This RSF was then used to calculate the ^{25}Mg fluence actually implanted into the glass (equation 2). As the ^{24}Mg and ^{25}Mg measurements in the glass were done simultaneously, the concentration of Si cancels out in the calculation. The calibration revealed that the real fluence was ~13% lower (2.61×10^{13} ions cm^{-2}) than its nominal value (3.0×10^{13} ions cm^{-2}) (K 02-2010_25Mg, Table 4). With this corrected value for the ^{25}Mg fluence, the simultaneously implanted Si wafer served as an absolutely calibrated Mg standard during our solar wind sample measurements. To design such an absolute calibration experiment a material has to be found that contains the element of interest as a trace amount (on the order of tens of ppm to 100 ppm) whose concentration is either accurately known or can be determined by other means and which is homogeneously distributed. The same technique can be applied to other elements, e.g., Ca, Cr, using other types of standard (NIST) glasses or minerals.

A different approach was required for calibrating the C and O fluence measurements, as these elements rarely occur as homogeneously distributed trace species in natural or artificial materials. Carbon and oxygen fluences were calibrated against ion implants conducted at CSNSM, Orsay. We used

SIDONIE for this purpose, an electromagnetic mass separator built for production of high purity targets for nuclear physic experiments (Chauvin et al., 2004). Carbon and oxygen implantation was performed at 40 keV with monocharged ions and molecules produced from source gases enriched in minor isotopes, ^{13}C and ^{18}O, by a hot cathode ion source. Implanted ion beams were mass separated in a large radius magnetic sector for isotopic purity. Three separate implantation experiments into Si were carried out for each isotope, ^{13}C and ^{18}O, involving single ions and molecules. For carbon, we implanted ^{13}C, $^{13}C^{18}O$, and $^{13}C^{16}O$ (Fig. 11), and for oxygen ^{18}O, $^{18}O^{18}O$, and $^{13}C^{18}O$. The purpose of this implantation scheme was to control the contribution of interfering molecules (e.g., hydrides) to the implanting beam and thus ensure a correct fluence. A single ion beam (e.g., ^{13}C) may contain some contribution of a molecule of the same mass (e.g., ^{12}CH); whereas molecule and, in particular, odd mass molecule ion beams (e.g. $^{13}C^{18}O$) show much cleaner spectra. The beam intensity was monitored by direct Faraday cup measurement at the mass focal plane and the total dose inferred with a precision of a few percent by the induced current measurement on the target holder. Potential interfering isotopes and molecules were shown to be negligible by high resolution mass scans performed before and after each implantation procedure. The doses (i.e. fluences) were determined from the time integrated current divided by the implanted surface (3.4 cm^2) with an accuracy of ~1%. The accuracy of the ^{18}O fluence in four of the Orsay implants was further cross-checked by Nuclear Reaction Analysis using the SAFIR beamline on the ALTAIS accelerator at Namur (Belgium). The bulk ^{18}O concentration at the sample surface was measured using the $^{18}O(p,\alpha)^{15}N$ reaction with a 740 keV proton beam, and a thin anodic $Ta_2^{18}O_5$ reference oxide (Amsel et al., 1978). The inferred ^{18}O fluence averaged over the four implants is $(1.09\pm0.02) \times 10^{15}$ ions cm^{-2} in agreement with the expected value within 1%. A SIMS traverse measured over the entire $^{13}C^{18}O$-implant (Fig. 11) confirmed homogeneous implantation with a spatial variability better than 0.8% (1 σ standard deviation; n= 12), that is within the range of reproducibility we achieved by the SIMS method. The average fluences measured by SIMS for three independent implantations of

37

^{13}C (i.e. ^{13}C, ^{13}C^{18}O, and ^{13}C^{16}O) as well as for ^{18}O (i.e. ^{18}O, ^{18}O^{18}O, and ^{13}C^{18}O) agree with the nominal values within ±0.5%.
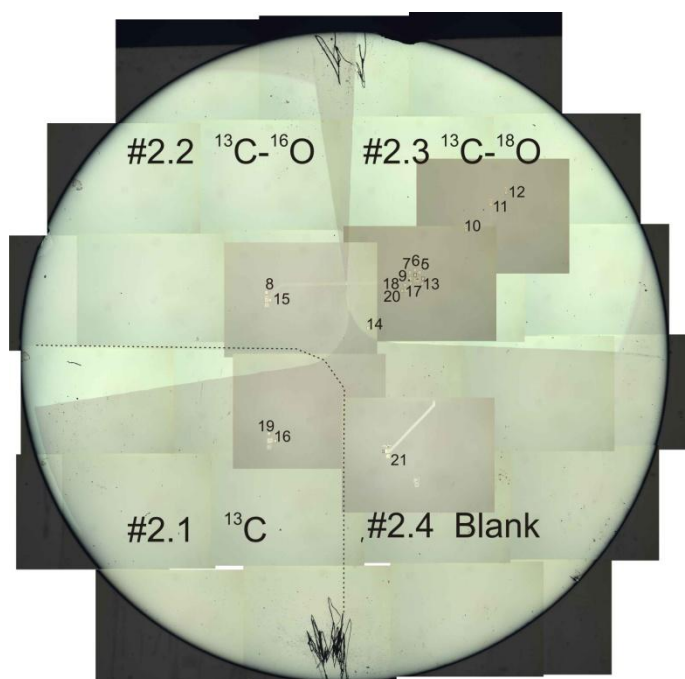
Fig. 11. Photomicrograph mosaic of the Si disk (2.54 cm in diameter) consecutively implanted with ^{13}C, ^{13}C^{18}O and ^{13}C^{16}O in quadrant 2.1, 2.3, and 2.2 respectively, quadrant 2.4 was left blank (i.e. shielded during implantation). Note, implants containing oxygen (#2.2 and #2.3) acquired a shaded aspect and appear light-gray in this photomicrograph. Superimposed to the image is a set of photomicrographs (their darker color is due to a different light exposure) depicting the sputter pits, including the traverse (upper right quadrant) across the ^{13}C^{18}O implant made to assess the homogeneity of the Orsay implants.

Table 4 intercompares the fluences of the various implant standards used in this study. For carbon and oxygen, fluences of the various implants were measured as unknowns relative to the Orsay implants adopted as the primary fluence standard, and deviations of Orsay-derived fluences from the nominal fluence are tabulated. Similarly, for Mg various implants are measured relative to the calibrated K 02-2010_25Mg implant. For nitrogen, the implant from facility B was adopted as the primary standard because of the good agreement between this facility and Orsay for carbon. For Na, Al, and Ca, for the

purposes of comparison, a recent implant from facility A is provisionally selected as the primary standard, pending an actual calibration; for Cr facility B. The relative sensitivity factors tabulated in Table 3 were calculated using the mentioned primary standards. Relative to the adopted primary standards, the nominal fluences are both high and low. There is also a tendency of older implants (e.g., facility C) to show larger and consistent discrepancies. Our examples show that the fluence of uncalibrated implants could be off by up to 20%, meaning that fluence calibration is essential for high accuracy analyses.

Table 4

Standard reference implants analyzed in this work.

Element	Implant name[1]	Implant facility	Implanted Isotope	Nominal fluence (10^{14} cm^{-2})	Calibrated fluence[2,4] (10^{14} cm^{-2})	% difference nominal - calibrated fluence	Energy (keV)	keV amu^{-1}
N	K 09-07_18O15N	A	^{15}N	10	11.5	13.2	45	3.0
	EAG 4257	B		10	10	0.0	100	6.7
	HR 9-99_ON	C		2.0	1.70	-17.4	15	1.0
	K 11-2012_15N100	A		10	10.3	3.0	100	6.7
C	LANL 5-05_13C	D	^{13}C	5.0	5.10	2.0	13	1.0
	K 8-08_13C	A		5.0	6.25	19.9	20	1.5
	EAG 4187	E		10	9.67	-3.4	50	3.8
	EAG 4257	B		10	10.2	1.8	88	6.8
	Orsay, 3 independent implants	CSNSM, Orsay		**10.92**	**10.92**	**0**	**16.8, 17.9, 40** [3]	**1.3 – 3.1**
O	K 09-07_18O15N	A	^{18}O	5.0	5.28	5.3	27	1.5
	K 8-08_18O	A		10	11.3	11.8	45	2.5
	HR 9-99_ON	C		2.0	1.74	-15.2	18	1
	EAG 4257	E		5.0	4.79	-4.3	107	5.9
	Orsay, 3 independent implants	CSNSM, Orsay		**10.93** / 10.99 (^{18}O^{18}O)	**10.93** / 10.99 (^{18}O^{18}O)	**0**	**20.0, 23.2, 40** [3]	**1.1 – 2.2**
Al	K 04-2013_AlCa	A	^{27}Al	0.10	0.10	0.0	80	3.0
	K 08-08_Al	A		0.10	0.0945	-5.8	40	1.5
Ca	K 04-2013_AlCa	A	^{42}Ca	0.10	0.10	0.0	120	2.9
	L26	C	^{40}Ca	0.30	2.50E+13	-19.9	200	5.0
Na	K 02-2013_Na25Mg	A	^{23}Na	0.10	0.10	0.0	100	4.3
	K 1987_Na(Stevie#194)	A		1.0	0.772	-29.6	100	4.3
Mg	K 02-2013_Na25Mg	A	^{25}Mg	0.10	0.0879	-13.8	100	4.0
	K 02-2010_25Mg	**A**		**(0.30)**	**0.261**	**0**	**75**	**3.0**
	K 02-2010_2526Mg	A		1.0	0.869	-15.1	75	3.0
	K 09-09_2526Mg	A		1.0	0.886	-12.9	75	3.0
	K 02-2010_2526Mg	A	^{26}Mg	1.0	0.908	-10.2	75	2.9
	K 09-09_2526Mg	A		1.0	0.911	-9.8	75	2.9
Cr	C 02-2013_62Ni52Cr	B	^{52}Cr	0.40	0.40	0.0	185	3.6
	L52	C		0.30	0.250	-20.0	80	1.5

[1] Most names include implanted isotopes and date of production

[2] C, O, and Mg implants printed in bold and marked by dark gray fields are absolutely calibrated and serve as the primary fluence standards; see text. Fluences of the other reference implants of the same element were calibrated against these implants.

[3] Implanted species for ^{13}C are ^{13}C^{18}O, ^{13}C^{16}O, ^{13}C and for ^{18}O: ^{18}O^{18}O, ^{13}C^{18}O, ^{18}O. Both ions and molecules were implanted at 40 keV total energy resulting in the given range of energies.

[4] Calibrations of the elements other than Mg, C and O are not available yet. We chose the implant whose nominal fluence may be close to the true fluence (marked by light gray fields) based on several factors (see text) and calculated the respective deviations to the other implant fluences.

7. Summary

We have documented in detail our approach of backside depth-profiling for quantitatively analyzing the fluences of shallowly implanted solar wind ions returned to Earth by the Genesis Discovery mission. The main analytical challenges overcome by this approach are: (1) unacceptable levels of mixing of residual surface contaminants into the solar wind signal and (2) the inability to quantify relative SIMS ion yields in the nonequilibrium sputtering regime which overlaps the implant profiles in the very near surface region of the Genesis collectors. By employing relatively low impact energy sputtering and well-constrained sample geometries, we can recover nearly complete depth profiles of implanted solar wind for several nonvolatile elements including Mg, Al, Ca, Cr, and to a lesser extent, Na. Measurements are possible in Genesis targets that collected solar wind from specific velocity regimes, in addition to the bulk solar wind. For volatile elements, including the abundant elements C, N, and O, it is possible to make measurements in bulk solar wind by backside profiling even though the in-depth profiles do not reach all the way to the original sample surface before becoming overwhelmed by terrestrial contamination. By careful modeling of the depth profile it is possible to obtain precise integrated depth profiles for all eight elements investigated here. The ion depth profiles can be quantified by use of appropriately calibrated ion implanted standards of these same elements into the same matrix target (Si, in all cases shown here). By these means it is possible to obtain accurate fluences of the solar wind ions collected during two years on space by the Genesis mission. The relation of the abundances of these elements in the solar wind to those in the Sun, and implications for solar physics and planetary cosmochemistry are discussed elsewhere.

Acknowledgements

References

Allton, J.H. et al., 2006. Genesis solar wind sample curation: A progress report., Lunar Planet. Sci. , Houston, USA, pp. #1611.

Allton, J.H., Wentworth, S.J., Rodriguez, M.C., Calaway, M.J., 2007. Cleaning Genesis solar wind collectors with ultrapure water: Residual contaminant particle analysis, Lunar Planet. Sci. , Houston, USA, pp. #2138

Amsel, G., Nadai, J.P., Ortega, C., Siejka, J., 1978. Precision absolute thin film standard reference targets for nuclear reaction microanalysis of oxygen isotopes: Part II: ^{18}O and ^{17}O standards. Nuclear Instruments and Methods in Physics Research, 149: 713-720.

Asplund, M., Grevesse, N., Sauval, A.J., Scott, P., 2009. The chemical composition of the Sun. Annu. Rev. Astron. Astrophys., 47: 481-522.

Burnett, D.S. et al., 2003. The Genesis discovery mission: Return of solar matter to earth. Space Sci. Rev., 105: 509-534.

Burnett, D.S. et al., 2014, in press. Ion Implants as Matrix-Appropriate Standards for Geochemical Ion Probe Analyses. Geostandards and Geoanal. Res.

Burnett, D.S., Team, G.S., 2011. Solar composition from the Genesis Discovery Mission. Proc. Nat. Acad. Sci., 108: 19147-19151.

Calaway, M.J. et al., 2007. Decontamination of Genesis array materials by UV ozone cleaning, Lunar Planet. Sci., Houston, USA, pp. #1627.

Calaway, M.J., Stansbery, E.K., Keller, L.P., 2009. Genesis capturing the sun: Solar wind irradiation at Lagrange 1. Nuclear Instruments & Methods in Physics Research Section B, 267: 1101-1108.

Cameca, 2004. Cameca IMS 1270/1280 User's Guide.

Chauvin, N., Dayras, F., Le Du, D., Meunier, R., 2004. SIDONIE: an electromagnetic isotope separator for preparation of high purity thin targets. Nucl. Instr. & Meth. in Phys. Res., Sect. A, 521: 149-155.

Eggins, S.M., Shelley, J.M.G., 2002. Compositional heterogeneity in NIST SRM 610-617 glasses. Geostandards and Geoanal. Res., 26: 269-286.

Fujiyama, N. et al., 2011. A beneficial application of backside SIMS for the depth profiling characterization of implanted silicon. Surface and Interface Analysis, 43: 654-656.

Giammanco, C., Wurz, P., Karrer, R., 2008. Minor ion abundances in the slow solar wind. ApJ, 681: 1703-1707.

Heber, V.S. et al., 2012a. Isotopic mass fractionation of solar wind: Evidence from fast and slow solar wind collected by the Genesis mission. ApJ, 759: 121-133.

Heber, V.S. et al., 2013. Carbon, nitrogen, and oxygen abundances in the solar wind and calibration of absolute abundances, Lunar Planet. Sci., The Woodlands, USA, pp. # 2540.

Heber, V.S. et al., 2012b. Magnesium isotopic composition of solar wind as test for isotopically fractionated solar wind, Lunar Planet. Sci. , The Woodlands, USA, pp. #2921.

Heber, V.S., McKeegan, K., Bochsler, P., Duprat, J., Burnett, D.S., 2014. The elemental composition of solar wind with implications for fractionation processes during solar wind formation, 45th Lunar Planet. Sci. Conf., The Woodlands, USA, pp. #2117.

Huss, G.R., Nagashima, K., Jurewicz, A.J.G., Burnett, D.S., Olinger, C.T., 2012. The isotopic composition and fluence of solar-wind nitrogen in a genesis B/C array collector. Meteoritics & Planet. Sci., 47: 1436-1448.

Jackman, J.A. et al., 1990. Back-side SIMS profiles of dopant redistribution under silicide films. Surface and Interface Analysis, 15: 451-453.

Jurewicz, A.J.G. et al., 2003. The Genesis solar-wind collector materials. Space Sci. Rev., 105: 535-560.

Leta, D.P., Morrison, G.H., 1980. Ion implantation for *in situ* quantitative ion microprobe analysis. Analytical Chemistry, 52: 277-280.

Marty, B., Chaussidon, M., Wiens, R.C., Jurewicz, A.J.G., Burnett, D.S., 2011. A ^{15}N-poor isotopic composition for the solar system as shown by Genesis solar wind samples. Science, 332: 1533-1536.

Marty, B. et al., 2010. Nitrogen isotopes in the recent solar wind from the analysis of Genesis targets: Evidence for large scale isotope heterogeneity in the early solar system. Geochimica Cosmochimica Acta, 74: 340-355.

McKeegan, K.D. et al., 2011. The oxygen isotopic composition of the Sun inferred from captured solar wind. Science, 332: 1528-1532.

Reed, W.P., 1992. Certificates of analysis for SRMs 610-611; 612-613; 614-615; 616-617 (Revised). National Institute of Standards and Technology, Gaithersburg, (USA).

Reisenfeld, D.B. et al., 2013. Solar wind conditions and composition during the Genesis mission as measured by in situ spacecraft. Space Sci. Rev., 175: 125-164.

Rieck, K.D., Jurewicz, A.J.G., Burnett, D.S., Hervig, R., 2014. Internally standardized measurements of solar wind sodium and potassium in Genesis diamond-like carbon collectors, Lunar Planet. Sci., The Woodlands, USA, pp. # 1758.

Slodzian, G., 1980. Microanalyzers using secondary ion emission. Advances in electronics and electron physics 138: 1-44.

von Steiger, R. et al., 2000. Composition of quasi-stationary solar wind flows from Ulysses/ Solar Wind Ion Composition Spectrometer. J. Geophys. Res., 105(A12): 27217-27238.

Wiens, R.C. et al., 2013. The Genesis Solar Wind Concentrator: Flight and post-flight conditions and modeling of instrumental fractionation Space Sci. Rev., 175: 93-124.

Wilson, R.G., Stevie, F.A., Magee, C.W., 1989. Secondary ion mass spectrometry: A practical handbook for depth profiling and bulk impurity analysis. John Wiley & Sons.

Yeo, K.L., Wee, A.T.S., Liu, R., Ng, C.M., See, A., 2002. SIMS backside depth profiling of ultra shallow implants using silicon-on-insulator substrates. Surface and Interface Analysis, 33: 373-375.

Yeo, K.L., Wee, A.T.S., See, A., Liu, R., Ng, C.M., 2003. SIMS backside depth profiling of ultra shallow implants. Applied Surface Science, 203-204: 335-338.

Ziegler, J.F., 2004. SRIM-2003. Nucl. Instr. Meth. Phys. Res., 219/220: 1027-1036.

Zinner, E., 1983. Sputter depth profiling of microelectronic structures. J.Electrochemical Soc., 130: 199C-222C.

Highlights

- report a method to analyze solar wind (SW)captured during the GENESIS mission

- Backside depth-profiling by secondary ion mass spectrometry (SIMS) was used

- Nearly complete depth profiles of implanted SW were obtained

- We present quantitative analyses of SW fluences for several elements